PNAS
www.pnas.org

**Supplementary Information for**

# A 4565 Myr old andesite from an extinct chondritic protoplanet.

Jean-Alix Barrat, Marc Chaussidon, Akira Yamaguchi, Pierre Beck, Johan Villeneuve, David J. Byrne, Michael W. Broadley, Bernard Marty

Corresponding author: Jean-Alix Barrat

Email: barrat@univ-brest.fr

**This PDF file includes:**

Supplementary Information Text, figures, and tables

## A/ Petrography, mineralogy, geochemistry, geochronology

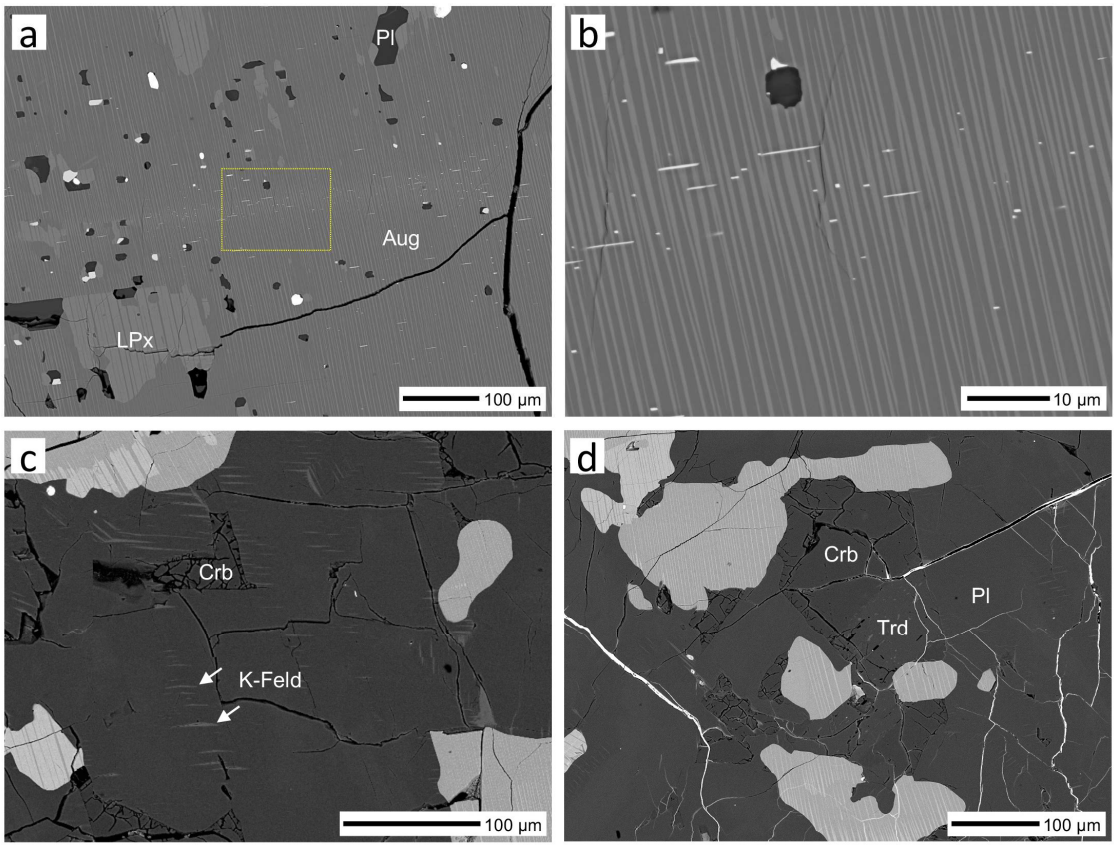


**Figure S1.** Back-scattered electron (BSE) images of EC 002. (a) Groundmass pyroxene composed of relict augite (Aug) and minor low-Ca pyroxene (LPx). Small inclusions of plagioclase (dark gray) and oxide minerals (white) occur. (b) Enlarged view of the dotted square in (a). Notice closely-spaced augite (medium gray) and low Ca-pyroxene lamellae (light gray). (c) Thin lamellae of K-feldspar (light gray) in plagioclase. (d) Cristobalite (Crb) and tridymite (Trd). Cristobalite is slightly fractured. Tridymite is slightly brighter under BSE and has fine inclusions of plagioclase.

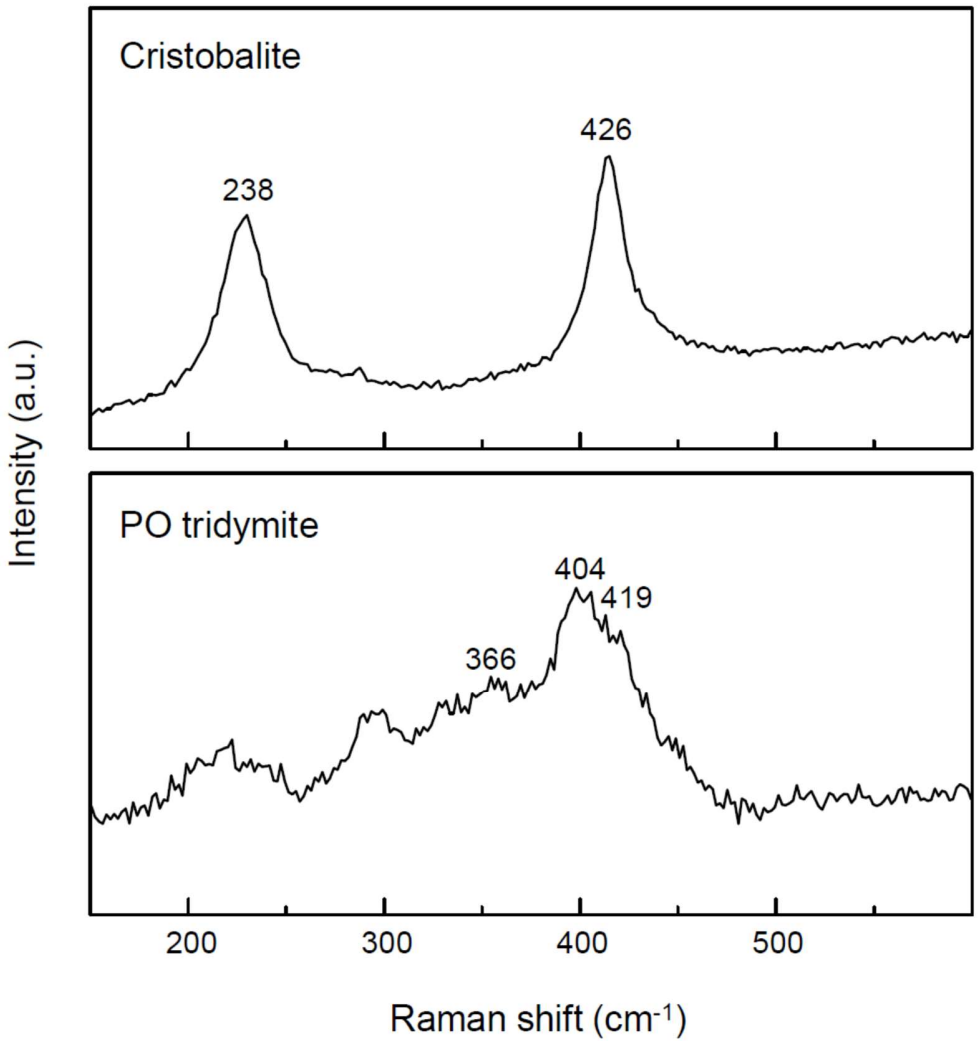


**Figure S2.** Representative Raman spectra of silica in EC 002**.**

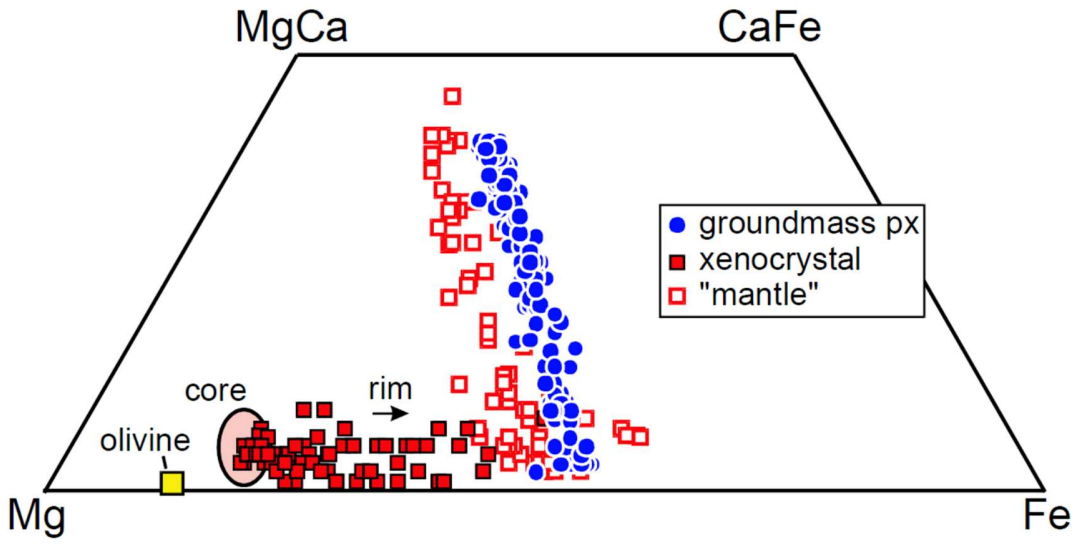


**Figure S3.** Olivine (megacryst) and pyroxene compositions. Groundmass pyroxenes are low-Ca pyroxene and augite. The intermediate Wo contents are due to incomplete spatial resolutions of electron microprobe.

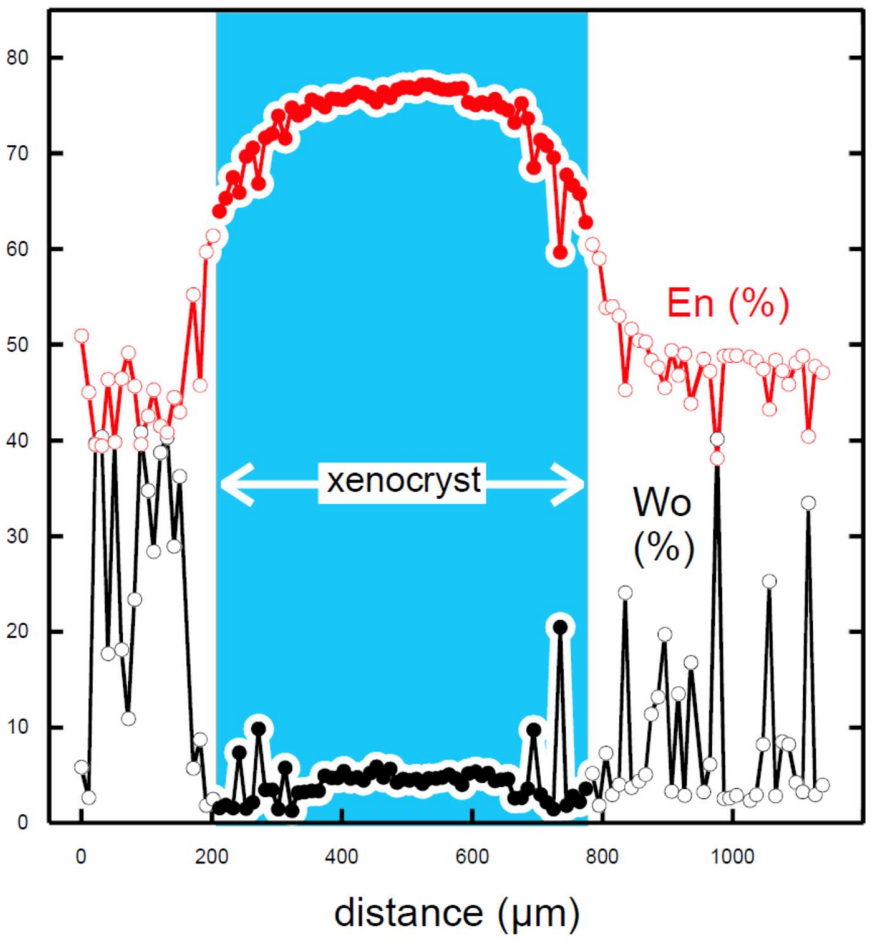


**Figure S4**. Chemical zoning (enstatite and wollastonite component, in mol%) of a small orthopyroxene xenocryst mantled by groundmass pyroxenes.

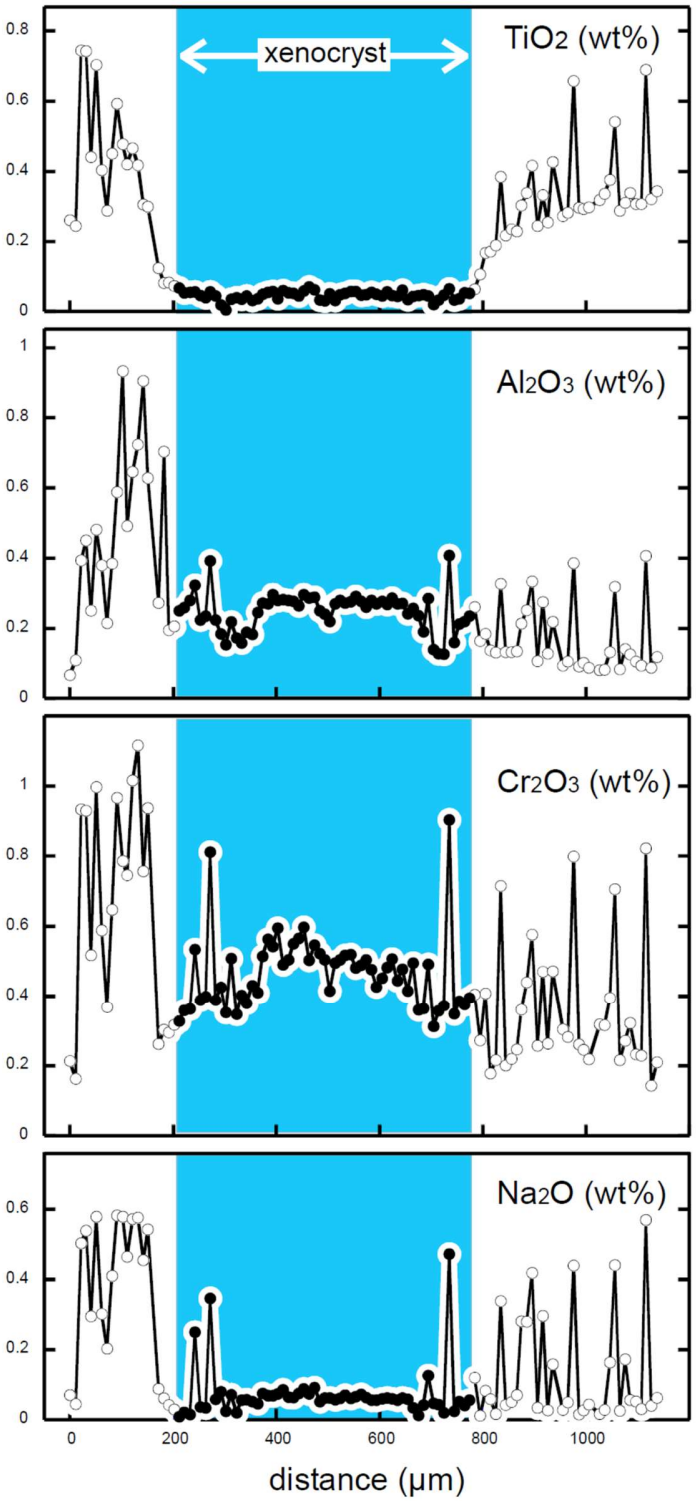


**Figure S5**. Chemical zoning ($TiO_2$, $Al_2O_3$, $Cr_2O_3$ and $Na_2O$ in wt%) of a small orthopyroxene xenocryst mantled by groundmass pyroxenes.

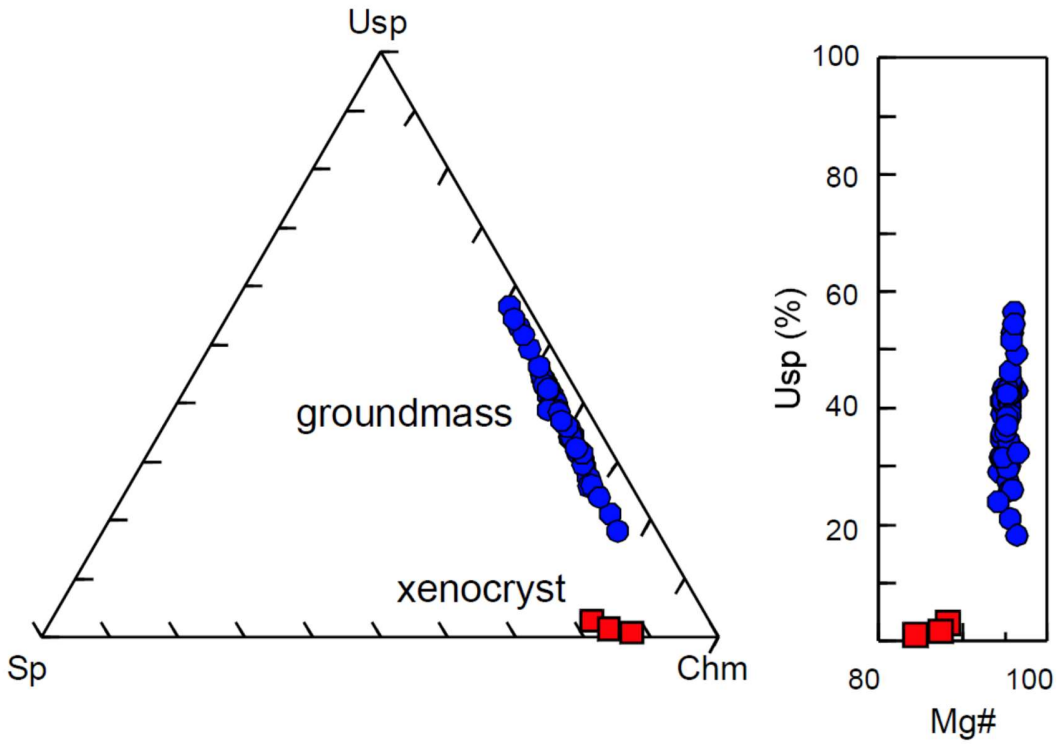


**Figure S6**. Spinel compositions.

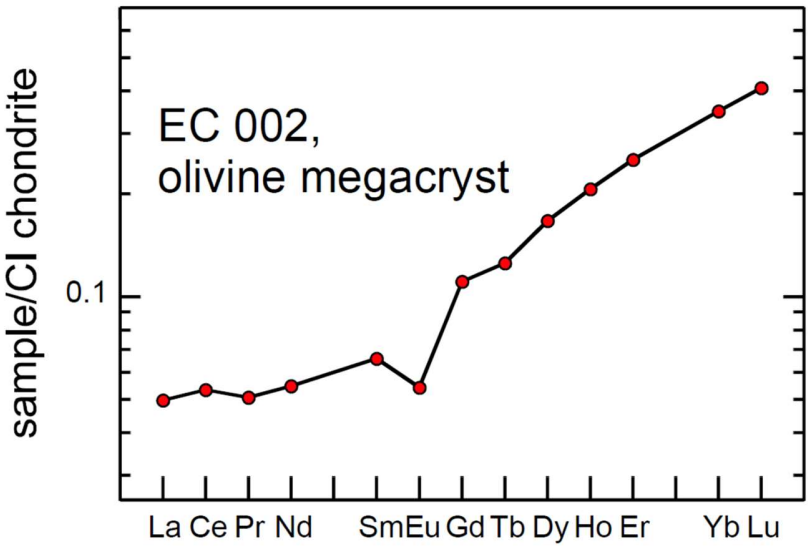


**Figure S7.** REE pattern of an olivine megacryst found in EC 002.

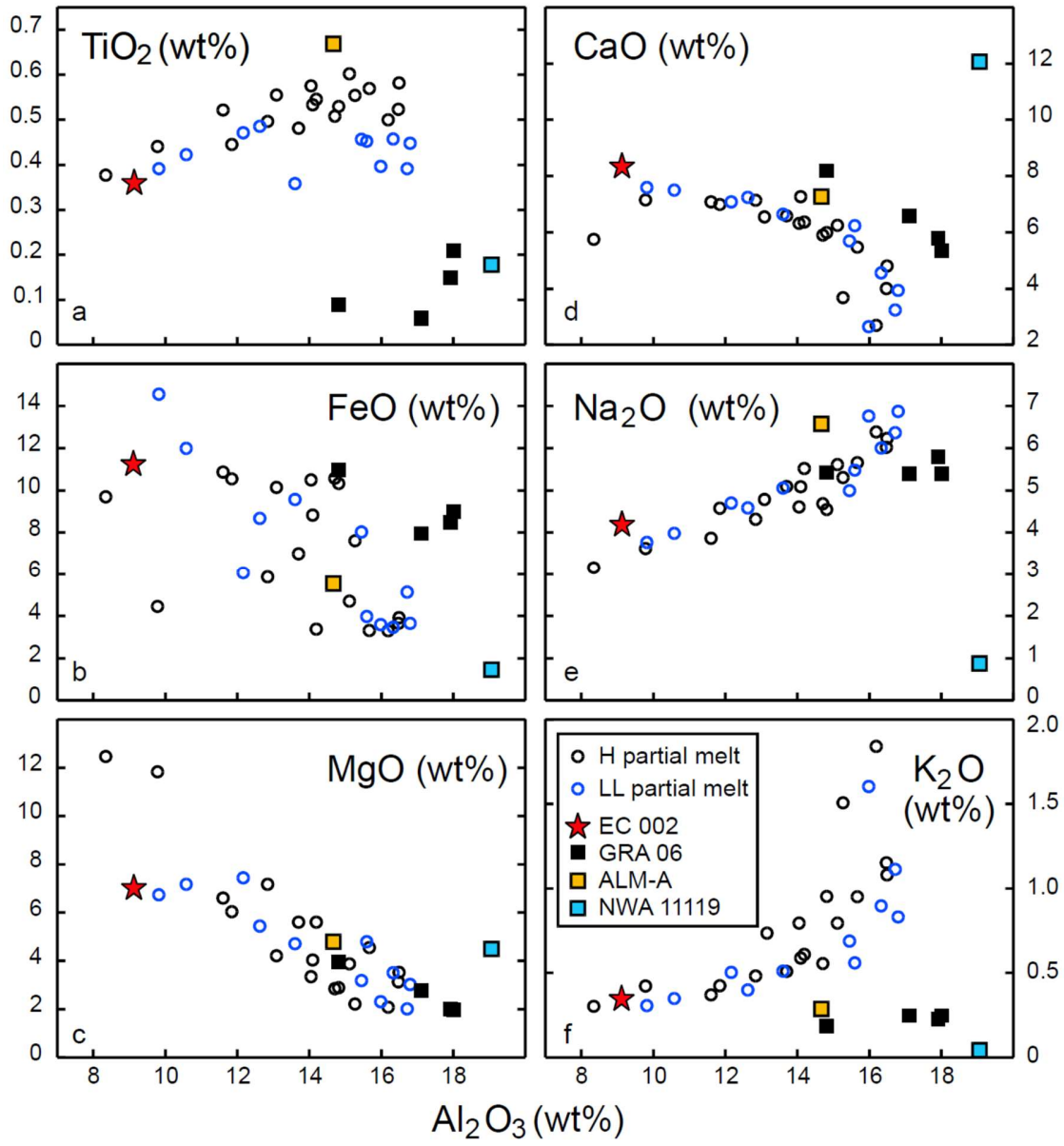


**Figure S8**. Compositions of EC 002 (this work) and other andesitic achondrites (1-3) compared with experimental partial melts from system with H or LL-chondrite compositions (4).

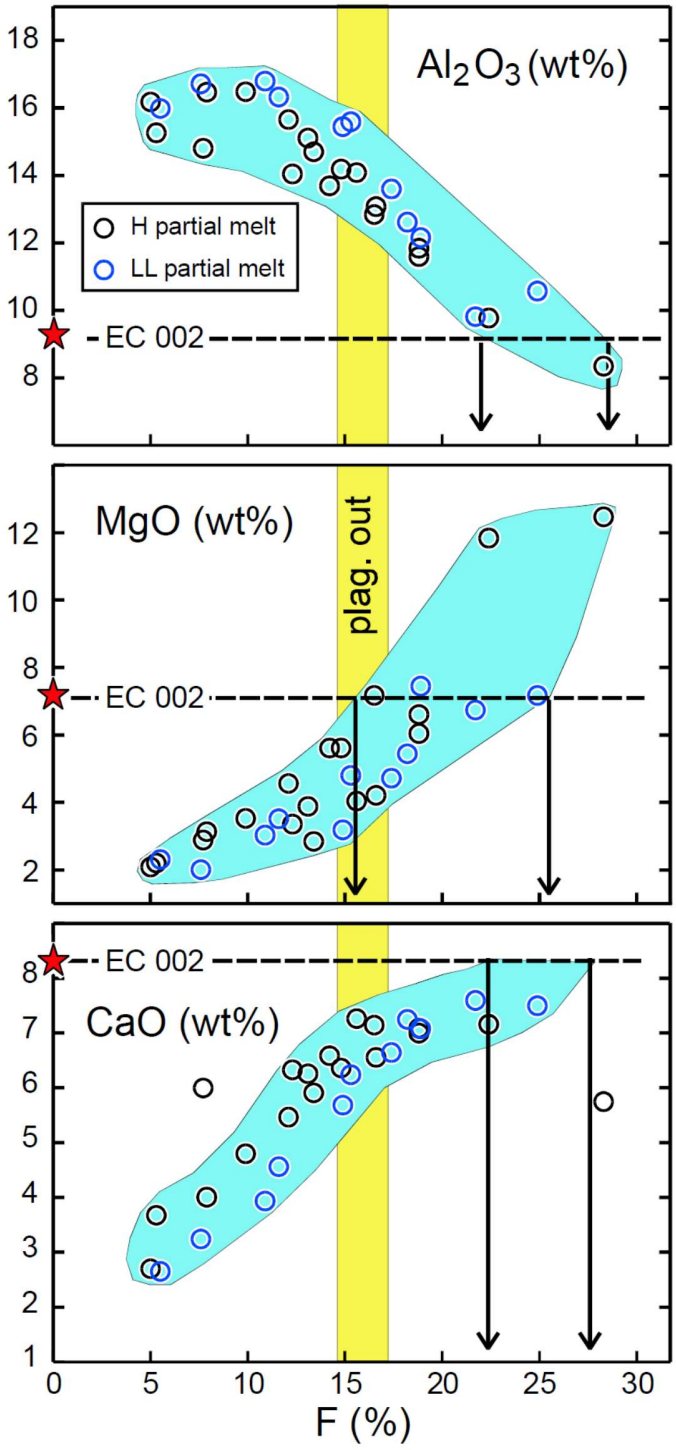


**Figure S9**. Compositions of EC 002 (this work) compared with experimental partial melts from system with H or LL-chondrite compositions (4). The composition of EC 002 suggests high melting degrees (F) around 25%.

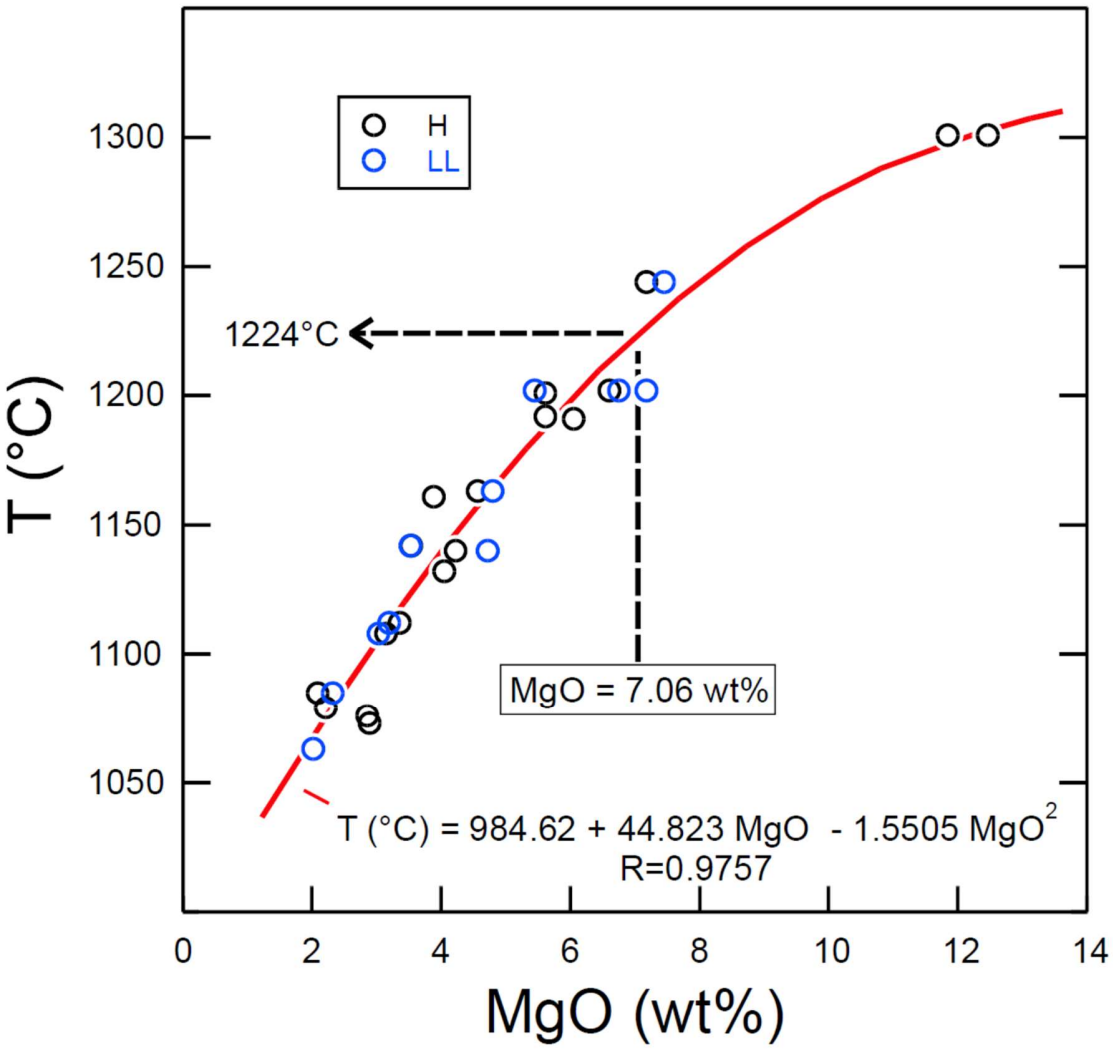


**Figure S10**. Liquidus temperature vs. MgO (wt%) for experimental melts obtained by partial melting from system with H or LL-chondrite compositions (4). The data are well described by a simple polynomial expression with errors < 20°C. A liquidus temperature of 1224°C is estimated for EC 002 (MgO=7.06 wt%).

**Table S1**. Representative compositions of pyroxenes and oxides in EC 002 (in wt%, n.d.: not determined).

| | $SiO_2$ | $TiO_2$ | $Al_2O_3$ | $Cr_2O_3$ | FeO | MnO | MgO | CaO | $Na_2O$ | $V_2O_3$ | NiO | ZnO | Total | | | |
|---|---|---|---|---|---|---|---|---|---|---|---|---|---|---|---|---|
| **Pyroxene** | | | | | | | | | | | | | | | | |
| Groundmass | | | | | | | | | | | | | | Wo | En | Fs |
| Low-Ca | 51.24 | 0.32 | 0.09 | 0.12 | 30.4 | 1.34 | 15.2 | 1.44 | 0.03 | n.d. | n.d. | n.d. | 100.16 | 3.12 | 45.57 | 51.31 |
| High-Ca | 51.87 | 0.27 | 0.96 | 1.17 | 13.6 | 0.64 | 12.1 | 18.6 | 0.54 | n.d. | n.d. | n.d. | 99.66 | 40.46 | 36.50 | 23.03 |
| Xenocryst | | | | | | | | | | | | | | | | |
| Core | 55.43 | 0.06 | 0.28 | 0.52 | 12.2 | 0.59 | 28.5 | 2.40 | 0.06 | n.d. | n.d. | n.d. | 100.05 | 4.65 | 76.89 | 18.47 |
| Rim | 51.91 | 0.24 | 0.13 | 0.22 | 27.2 | 1.25 | 17.1 | 2.06 | 0.05 | n.d. | n.d. | n.d. | 100.16 | 4.38 | 50.46 | 45.16 |
| | | | | | | | | | | | | | | | | |
| **Spinel** | | | | | | | | | | | | | | Usp | Sp | Cm |
| Low-Ti | 0.04 | 6.38 | 2.59 | 50.74 | 36.6 | 1.25 | 0.77 | 0.19 | <0.01 | 0.44 | <0.03 | <0.02 | 98.61 | 18.19 | 5.79 | 76.02 |
| High-Ti | 0.04 | 20.1 | 1.19 | 27.67 | 48.8 | 0.91 | 1.13 | <0.01 | <0.01 | 0.23 | <0.03 | 0.04 | 99.84 | 56.47 | 2.63 | 40.90 |
| | | | | | | | | | | | | | | | | |
| **Ilmenite** | | | | | | | | | | | | | | | | |
| Average | <0.02 | 53.9 | <0.01 | 0.20 | 44.13 | 1.07 | 1.64 | <0.01 | <0.01 | <0.03 | <0.03 | 0.01 | 100.99 | | | |
| *1SD, n=9* | | *0.42* | | *0.08* | *0.58* | *0.07* | *0.20* | | | | | *0.01* | | | | |

**Table S2**. Compositions of bulk pyroxenes (in wt%, n= number of analyses).

| | n | $SiO_2$ | $TiO_2$ | $Al_2O_3$ | $Cr_2O_3$ | FeO | MnO | MgO | CaO | $Na_2O$ | Total | Wo | En | Fs |
|---|---|---|---|---|---|---|---|---|---|---|---|---|---|---|
| **Groundmass pyrox.** | | | | | | | | | | | | | | |
| P3-1 | 21 | 52.0 | 0.40 | 0.68 | 0.83 | 17.6 | 0.79 | 12.1 | 15.1 | 0.47 | 100.0 | 32.99 | 36.93 | 30.08 |
| | *1SD* | *0.3* | *0.17* | *0.27* | *0.15* | *1.2* | *0.05* | *0.4* | *1.0* | *0.10* | | | | |
| P3-2 | 44 | 51.6 | 0.59 | 0.51 | 0.73 | 19.2 | 0.85 | 12.3 | 13.7 | 0.40 | 99.9 | 29.99 | 37.33 | 32.69 |
| | *1SD* | *0.6* | *0.09* | *0.15* | *0.10* | *1.7* | *0.07* | *0.4* | *1.7* | *0.05* | | | | |
| P-4 | 15 | 51.9 | 0.34 | 0.89 | 0.86 | 17.9 | 0.79 | 12.2 | 14.2 | 0.51 | 99.7 | 31.47 | 37.53 | 31.00 |
| | *1SD* | *1.1* | *0.09* | *0.50* | *0.17* | *2.9* | *0.11* | *0.7* | *2.9* | *0.24* | | | | |
| P-5 | 20 | 51.9 | 0.35 | 1.88 | 1.16 | 18.5 | 0.81 | 11.9 | 12.0 | 0.92 | 99.4 | 27.71 | 38.52 | 33.77 |
| | *1SD* | *2.7* | *0.28* | *2.92* | *1.48* | *3.1* | *0.14* | *1.8* | *3.4* | *1.31* | | | | |
| P-6 | 20 | 51.9 | 0.42 | 0.76 | 0.90 | 18.0 | 0.82 | 12.3 | 14.3 | 0.47 | 99.9 | 31.51 | 37.61 | 30.88 |
| | *1SD* | 0.6 | 0.13 | 0.29 | 0.30 | 2.0 | 0.08 | 0.5 | 2.0 | 0.13 | | | | |
| P-7 | 20 | 51.8 | 0.38 | 0.85 | 0.82 | 17.7 | 0.79 | 12.2 | 14.4 | 0.48 | 99.5 | 31.51 | 37.61 | 30.88 |
| | *1SD* | *0.9* | *0.10* | *0.48* | *0.13* | *1.4* | *0.06* | *0.5* | *1.1* | *0.18* | | | | |
| **Xenocryst core** | | | | | | | | | | | | | | |
| | 6 | 55.5 | 0.03 | 0.28 | 1.02 | 12.15 | 0.58 | 28.21 | 2.40 | 0.06 | 100.2 | 4.69 | 76.77 | 18.54 |
| | *1SD* | *0.5* | *0.01* | *0.03* | *0.45* | *0.25* | *0.01* | *0.44* | *0.52* | *0.02* | | | | |

**Table S3**. Chemical compositions of feldspars and silica (in wt%).

| | $SiO_2$ | $TiO_2$ | $Al_2O_3$ | $Cr_2O_3$ | FeO | MnO | MgO | CaO | $Na_2O$ | $K_2O$ | Total | Or | Ab | An |
|---|---|---|---|---|---|---|---|---|---|---|---|---|---|---|
| **Feldspar** | | | | | | | | | | | | | | |
| Low-Na | 63.2 | <0.03 | 23.0 | <0.03 | 0.08 | <0.03 | <0.03 | 4.45 | 8.63 | 0.47 | 99.8 | 2.69 | 75.75 | 21.55 |
| High-Na | 66.7 | 0.09 | 20.3 | <0.03 | 0.17 | <0.03 | <0.03 | 1.40 | 9.90 | 1.23 | 99.8 | 7.04 | 86.22 | 6.74 |
| High-K | 64.3 | 0.12 | 18.8 | 0.03 | 0.31 | <0.03 | <0.03 | 0.87 | 1.26 | 14.3 | 100.0 | 84.39 | 11.31 | 4.30 |
| **Silica minerals** | | | | | | | | | | | | | | |
| 1 | 95.9 | 0.21 | 2.48 | 0.02 | 0.04 | <0.03 | <0.03 | 0.09 | 1.20 | 0.01 | 100.0 | | | |
| 2 | 95.8 | 0.20 | 1.87 | <0.03 | 0.05 | <0.03 | <0.03 | 0.04 | 0.77 | 0.42 | 99.2 | | | |

**Table S4**. Bulk chemical composition of EC 002 and of an olivine megacryst (oxydes in wt%, trace elements in µg/g, n.d. = not determined).

| | W.R. | olivine | | W.R. | olivine | | W.R. | olivine |
|---|---|---|---|---|---|---|---|---|
| $SiO_2$ | 58.01 | (38.53) | Li | 3.59 | n.d. | Sm | 0.833 | 0.0101 |
| $TiO_2$ | 0.36 | 0.09 | Be | 0.122 | 0.007 | Eu | 0.342 | 0.00318 |
| $Al_2O_3$ | 9.12 | 1.66 | P | 216 | < 10 | Gd | 1.16 | 0.0228 |
| $Cr_2O_3$ | 0.42 | 1.00 | K | 3057 | 102 | Tb | 0.222 | 0.00470 |
| FeO | 11.22 | 11.11 | Sc | 30.49 | 9.90 | Dy | 1.52 | 0.0423 |
| MnO | 0.47 | 0.46 | Ti | 2309 | 303 | Ho | 0.339 | 0.0117 |
| MgO | 7.06 | 45.88 | V | 97.0 | 98.7 | Er | 1.01 | 0.0418 |
| CaO | 8.31 | 1.27 | Mn | 3289 | 3703 | Tm | 0.152 | n.d. |
| $Na_2O$ | 4.20 | n.d. | Co | 5.85 | 10.15 | Yb | 0.984 | 0.0586 |
| $K_2O$ | 0.34 | n.d. | Ni | 18.49 | 1.31 | Lu | 0.147 | 0.0100 |
| $P_2O_5$ | 0.06 | n.d. | Cu | 1.35 | 0.05 | Hf | 0.563 | 0.00491 |
| total | 99.58 | (100) | Zn | 0.44 | 0.09 | Ta | 0.0726 | n.d. |
| | | | Ga | 2.60 | 0.13 | W | 0.022 | n.d. |
| Mg# | 52.87 | 88.04 | Rb | 8.60 | 4.88 | Pb | 0.090 | 0.0048 |
| | | | Sr | 58.45 | 0.44 | Th | 0.136 | n.d. |
| CIPW norm | | | Y | 9.55 | 0.357 | U | 0.109 | 0.001 |
| qz | 2.51 | | Zr | 18.96 | 0.301 | | | |
| pl | 40.57 | | Nb | 1.61 | 0.040 | $La_n/Sm_n$ | 0.94 | 0.75 |
| or | 2.01 | | Cs | 0.293 | 0.284 | $Gd_n/Lu_n$ | 0.95 | 0.27 |
| di | 29.78 | | Ba | 47.51 | 0.198 | Eu/Eu* | 1.05 | 0.63 |
| hy | 23.27 | | La | 1.20 | 0.0117 | Tm/Tm* | 0.973 | - |
| il | 0.68 | | Ce | 3.14 | 0.0320 | Zr/Hf | 33.68 | 61.30 |
| ap | 0.14 | | Pr | 0.475 | 0.00461 | Nb/Ta | 22.18 | - |
| chr | 0.62 | | Nd | 2.46 | 0.0254 | | | |

**Table S5.** Al-Mg data for EC 002 plagioclases.

| | $^{27}Al/^{24}Mg$ | 2SE | $\delta^{25}Mg$ | 2SE | $\delta^{26}Mg$ | 2SE | $\delta^{26}Mg^*$ | 2SE |
|---|---|---|---|---|---|---|---|---|
| plag#1 | 4262 | 136 | 16 | 2.3 | 202.7 | 2.2 | 172 | 5.0 |
| plag#2 | 1597 | 142 | 7.2 | 2.3 | 79.0 | 2.8 | 65.2 | 5.2 |
| plag#3 | 4867 | 152 | 12.3 | 2.4 | 223.8 | 3.2 | 200.2 | 5.7 |
| plag#5 | 3427 | 182 | 10.1 | 2.4 | 164.3 | 3.7 | 144.9 | 6.0 |
| plag#6 | 2066 | 182 | 9.7 | 2.4 | 103.1 | 4.1 | 84.6 | 6.2 |
| plag#7 | 3983 | 138 | 11.9 | 2.3 | 188.4 | 2.2 | 165.5 | 5.1 |
| plag#8 | 4661 | 161 | 11.2 | 2.5 | 215.1 | 3.2 | 193.6 | 5.9 |
| plag#9 | 3372 | 162 | 11.9 | 2.5 | 160.4 | 3.9 | 137.5 | 6.2 |
| plag#10 | 2893 | 169 | 11.0 | 2.5 | 134.1 | 2.7 | 112.9 | 5.5 |
| plag#11 | 3039 | 141 | 7.0 | 2.4 | 142.7 | 2.1 | 129.2 | 5.1 |
| plag#14 | 4586 | 136 | 10.9 | 3.0 | 207.8 | 2.5 | 186.9 | 6.3 |
| plag#15 | 5316 | 158 | 11.5 | 2.5 | 237.3 | 2.4 | 215.2 | 5.5 |
| plag#16 | 4926 | 147 | 13.1 | 2.4 | 223.1 | 3.3 | 197.9 | 5.6 |
| plag#17 | 3275 | 141 | 11.2 | 2.2 | 159.6 | 2 | 138.1 | 4.7 |
| plag#18 | 4469 | 141 | 10.0 | 2.6 | 207.4 | 1.9 | 188.3 | 5.5 |
| plag#19 | 5310 | 152 | 13.6 | 3.0 | 240.8 | 2.9 | 214.6 | 6.5 |
| plag#20 | 3930 | 140 | 10.5 | 2.6 | 183.4 | 2.1 | 163.3 | 5.5 |
| plag#21 | 3097 | 172 | 10.4 | 2.7 | 143.5 | 3.8 | 123.6 | 6.5 |
| plag#22 | 1949 | 145 | 5.8 | 1.5 | 91.7 | 2.4 | 80.5 | 3.7 |

**Table S6.** Al-Mg data for EC 002 pyroxenes.

| | $^{27}Al/^{24}Mg$ | 2SE | $\delta^{25}Mg$ | 2SE | $\delta^{26}Mg$ | 2SE | $\delta^{26}Mg^*$ | 2SE |
|---|---|---|---|---|---|---|---|---|
| px #1 | 0.0362 | 0.0001 | 1.40 | 0.07 | 2.62 | 0.07 | -0.08 | 0.15 |
| px #2 | 0.0633 | 0.0001 | 1.52 | 0.07 | 2.90 | 0.07 | -0.02 | 0.15 |
| px #3 | 0.0350 | 0.0001 | 1.33 | 0.06 | 2.72 | 0.06 | 0.16 | 0.14 |
| px #4 | 0.0223 | 0.0001 | 1.45 | 0.06 | 2.69 | 0.07 | -0.10 | 0.14 |
| px #5 | 0.0233 | 0.0001 | 1.40 | 0.06 | 2.92 | 0.07 | 0.22 | 0.14 |
| px #6 | 0.0330 | 0.0001 | 1.66 | 0.06 | 3.21 | 0.07 | 0.02 | 0.14 |
| px #7 | 0.0438 | 0.0001 | 1.28 | 0.07 | 2.45 | 0.07 | -0.02 | 0.16 |
| px #8 | 0.0448 | 0.0001 | 1.24 | 0.06 | 2.57 | 0.07 | 0.19 | 0.14 |
| px #9 | 0.0425 | 0.0001 | 1.27 | 0.06 | 2.68 | 0.07 | 0.25 | 0.14 |
| px #10 | 0.0776 | 0.0001 | 1.29 | 0.08 | 2.65 | 0.08 | 0.14 | 0.17 |
| px #11 | 0.0261 | 0.0001 | 1.47 | 0.05 | 2.84 | 0.07 | -0.03 | 0.13 |
| average | 0.0407 | 0.0102 | 1.39 | 0.08 | 2.75 | 0.13 | 0.067 | 0.076 |

**Table S7.** Noble gas abundances and isotope ratios for EC 002. Gas was extracted by step heating sequentially to the temperatures indicated. Total isotope ratios are calculated as a weighted average to account for the differential release of gas at different stages of heating.

| | Abundances (mol) | | | | | | Isotope ratios | | | | | | | | | |
|---|---|---|---|---|---|---|---|---|---|---|---|---|---|---|---|---|
| T (°C) | $^{3}He$ (x$10^{18}$) | ±1σ | $^{21}Ne$ (x$10^{17}$) | ±1σ | $^{40}Ar$ (x$10^{14}$) | ±1σ | $^{3}He/^{4}He$ | ±1σ | $^{20}Ne/^{22}Ne$ | ±1σ | $^{21}Ne/^{22}Ne$ | ±1σ | $^{40}Ar/^{36}Ar$ | ±1σ | $^{38}Ar/^{36}Ar$ | ±1σ |
| 600 | 3374 | 227 | 67.0 | 3.1 | 14.8 | 0.7 | 0.00871 | 0.00007 | 0.571 | 0.003 | 0.613 | 0.013 | 1026 | 14 | 0.215 | 0.006 |
| 800 | 70160 | 4720 | 89.3 | 4.1 | 1417 | 45 | 0.00741 | 0.00007 | 0.506 | 0.003 | 0.675 | 0.014 | 19701 | 178 | 0.791 | 0.011 |
| 1000 | 862 | 58 | 69.2 | 3.2 | 1139 | 36 | 0.00601 | 0.00007 | 0.624 | 0.004 | 0.880 | 0.019 | 25096 | 236 | 0.997 | 0.014 |
| 1200 | 3907 | 262 | 1217 | 55 | 6390 | 198 | 0.00448 | 0.00003 | 0.807 | 0.003 | 0.870 | 0.018 | 4698 | 33 | 1.218 | 0.016 |
| 1400 | 5.9 | 0.6 | 7.6 | 0.4 | 77.5 | 2.5 | 0.00105 | 0.00011 | 0.613 | 0.014 | 0.767 | 0.019 | 492.5 | 4.3 | 0.395 | 0.005 |
| **Total** | 78310 | 4730 | 1450 | 56 | 9039 | 207 | 0.00731 | 0.00007 | 0.768 | 0.002 | 0.846 | 0.015 | 5522 | 41 | 1.170 | 0.015 |

**Concentration (mol/g)**

| $^{3}He$ | $^{21}Ne$ | $^{40}Ar$ |
|---|---|---|
| 9.55 (±0.57) x$10^{-12}$ | 1.77 (±0.07) x$10^{-12}$ | 1.10 (±0.03) x$10^{-8}$ |

**B/ Reflectance spectra of Erg Chech 002 and search for parent bodies.**

All spectra (Fig. S11) showed two strong absorptions around 1 µm (Band I) and 2 µm (Band II) diagnostic of pyroxene. The position of the two bands points toward the presence of clinopyroxene (5). In order to compare the spectra of EC 002 with asteroid observations, we calculated the Band Area Ratio (BAR (6)) and the position of Band I and BII.

***Space weathering model***- An ensemble of processes referred to as space weathering are known to act at the surface of airless bodies (7). These processes lead to a modification of the optical properties of surface material that may need to be accounted for in the comparison of spectra of meteorites to telescopic observations of small bodies. In the case of silicate-rich asteroids, the model of Hapke (8) enables to simulate numerically these effects, by modeling the incorporation of small opaque grains to the measured spectra. The Hapke model (8) was applied to the spectra of EC 002 powders, with different magnitude of space weathering, corresponding to different amounts of opaque phases incorporated in the silicate grains. The spectra resulting from these simulations are shown in figure S12 (top). These simulations reveal a progressive darkening and reddening of the spectra together with a decrease of the silicate absorptions (Figure S12 top).

***Spectral effects of adding olivine xenocrysts***- Because some samples of EC 002 contain olivine xenocrysts, we investigated numerically the effect of adding olivine crystals to the measured spectra of EC 002. For that, we used the model of Hapke (9). A reflectance spectra of San Carlos olivine of known grain size was used, and numerically mixed to the spectra of EC 002. Mixture were performed in single-scattering albedo space, in order to simulate the spectrum an intimate mixture. Results are shown in figure S12 bottom, in the cases of adding 5,10 and 20 vol. % of olivine to our measured EC 002 spectrum.

***Spectral effects of adding fragments of a residual mantle-*** In order to model the effect of mixing EC 002 with fragments of excavated mantle, we proceeded as follow. The mantle signature was calculated using reflectance spectra of olivine ($Fo_{90}$, RELAB database) mixed in equal proportion with orthopyroxene ($En_{80}$, RELAB database). The mixture of olivine and pyroxene was computed in single-scattering albedo space to model an intimated mixture. This calculated mantle spectrum was then mixed with the reflectance spectrum measured for EC 002 powder using a linear mixing model (Fig. S13).

***Comparison to taxonomic endmembers***- In figure S12 bottom, the spectra of EC 002 are compared to the spectra of asteroid taxonomic endmembers with strong pyroxene silicate signatures, namely O- and V- type asteroids (Fig S11 bottom). None of the taxonomic endmembers identified by DeMeo et al. (10) appears to correspond to the spectra measured for EC 002 (Fig S11 bottom). To push the comparison further, the BAR vs Band I position diagram can be used following Gaffey et al. (6). This analysis confirms the lack of spectral matches among taxonomic endmembers (Fig. S13). It also reveals that the spectra of EC 002 is distinct from that of HED meteorites, with a higher position of Band I, and a lower Band Area Ratio.

The models described earlier enables to draw the potential evolution of EC 002 in this diagram as a response of olivine addition or space-weathering. Space-weathering is not able to move the location of EC 002 toward any know taxonomic endmember. In the case of addition of olivine, the position of EC 002 moves close to the rare O-type endmember. However, the amount of olivine needed is quite high (20 %) when comparing to the typical amount of xenolitic olivine, when present. Note that O-type asteroids are extremely rare and include at the moment only a few objects.

***Comparison to Sloan Digital Sky Survey (SDSS)-*** Color surveys while less powerful in term of composition, offer the capability to observe several orders of magnitudes more objects than spectroscopy. Because of the strong absorption feature at 1-µm in the spectra of EC 002, color survey including an infrared filter enable to search for possible parent bodies within a much higher number of asteroids. For that, we followed the procedure describe in DeMeo and Carry (11) that was used to map the distribution of asteroids spectral types across the Solar System (12). We used data from the SDDS, selected following the same analysis as in DeMeo and Carry (11). Colors of EC 002 and different classes of meteorites were also computed and plot in the z-i vs g'r'i' slope diagram. Spectra of HED meteorites and ordinary chondrites were extracted through the RELAB database (13). This plot (Fig. S14) reveals that the colors of EC 002 lie outside of the asteroid endmember boundaries used in DeMeo and Carry (11) and that the vast majority of asteroids do not match the composition of Erg Chech. Space weathering can explain the mismatch of HED meteorites and V-type asteroids, but in the case of EC 002, space weathering models do not "push" the colors of EC 002 in one of the asteroid endmembers. As concluded from spectroscopy, color analysis furthers strength the lack of EC 002-like asteroid within the Solar System.

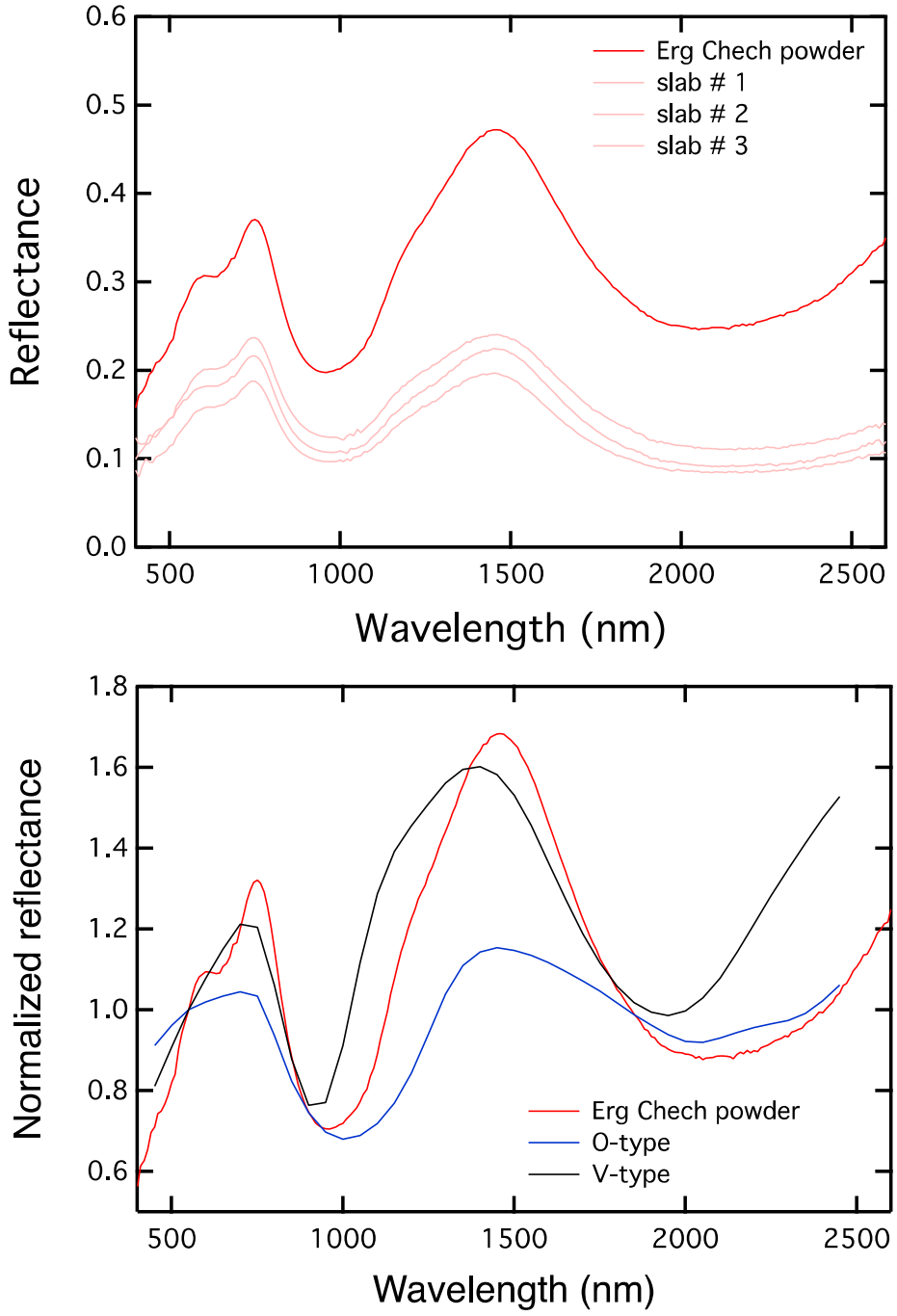


**Fig. S11**. Top) Reflectance spectra of EC 002 obtained for powdered sample, and 3 distinct locations of a raw piece of sample. Bottom) Reflectance spectra of EC 002 compared to V- and O- type endmembers (12)

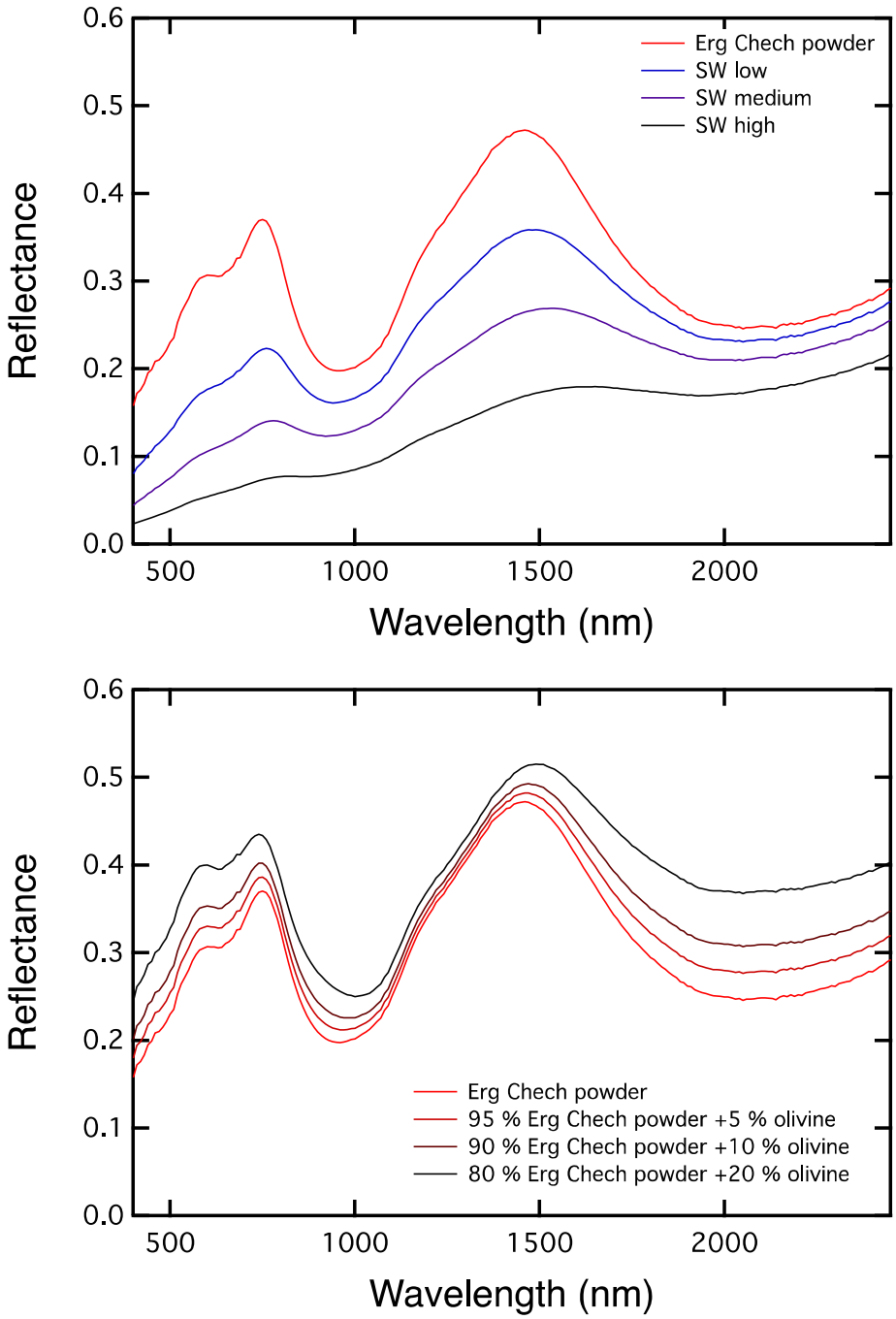


Fig. S12: Modeled spectra of EC 002 considering a space-weathering model (top) and mixture with olivine crystals (bottom)

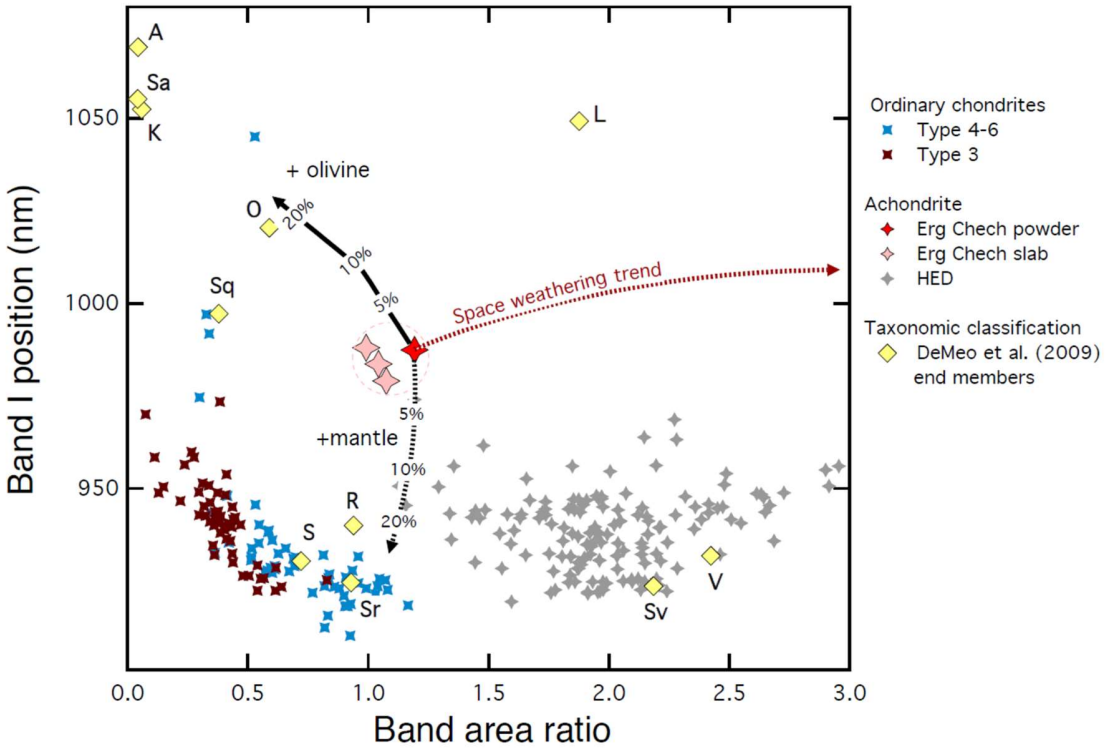


Fig. S13. BII/BI area ratio as a function of the Band I position. Parameters derived for EC 002 are compared to those of HED meteorites and ordinary chondrites (RELAB database). The positions of DeMeo et al. (11) asteroid endmembers are also shown, and the trends that were calculated based on mixtures with olivine, mantle, and using a space weathering model (8).

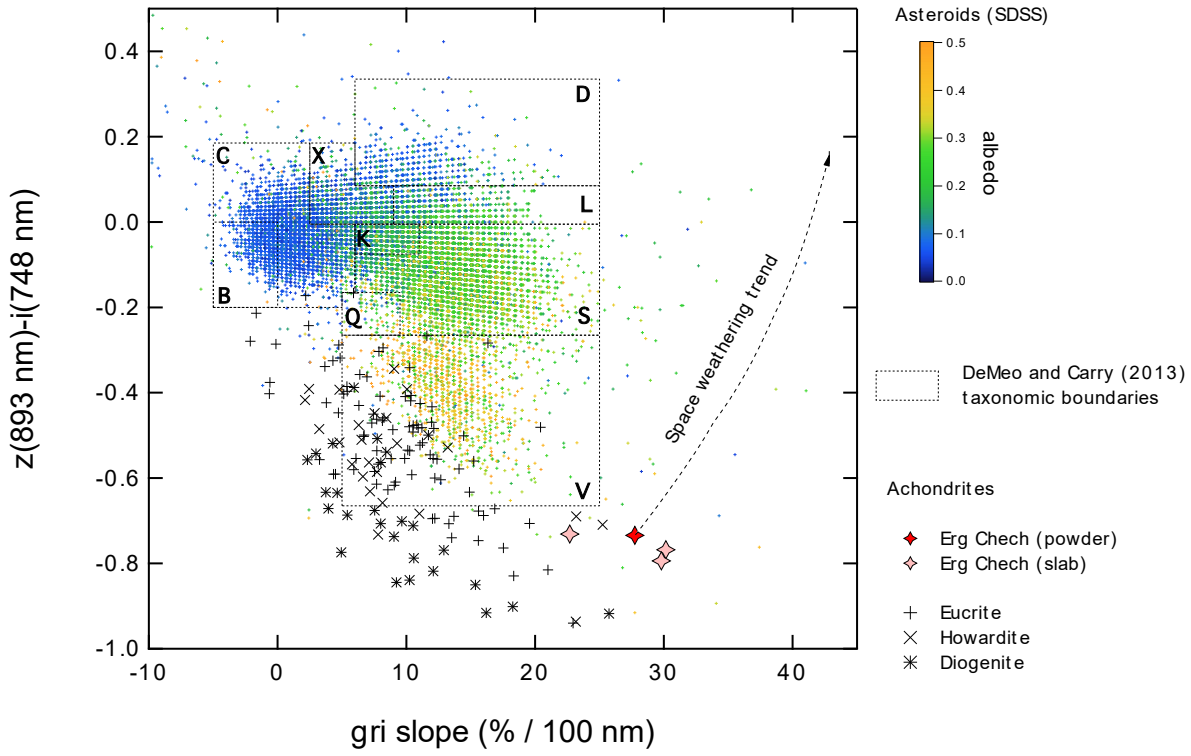


Fig. S14. Color diagram used by DeMeo and Carry (11) for classifying asteroid from the SDSS (asteroid are color coded here according to their wise albedo (13), compared to Erg Chech 002 and HED meteorite. This graph testifies of the scarcity of Erg Chech 002 -like objects, even if possible effects of space weathering are taken into account.

## SI References


1. J.M.D. Day, et al., Early formation of evolved asteroidal crust. *Nature* 457(7226), 179-182 (2009).
2. A. Bischoff, et al., Trachyandesitic volcanism in the early Solar System. *Proc. Natl. Acad. Sci. U.S.A.* 111, 12689-12692 (2014).
3. P. Srinivasan, *et al.*, Silica-rich volcanism in the early solar system dated at 4.565 Ga. *Nature Commun.* 9**,** 3036 (2018).
4. M. Collinet, T. L. Grove, Widespread production of silica- and alkali-rich melts at the onset of planetesimal melting. *Geochim. Cosmochim. Acta* 277, 334-357 (2020).
5. J. B. Adams, Visible and near-infrared diffuse reflectance spectra of pyroxenes as applied to remote sensing of solid objects in the solar system. *Journal of Geophysical Research* 79, 4829 (1974).
6. M. J. Gaffey et al., Mineralogy of Asteroids. *Asteroids III*, 183–204 (2002).
7. C. M. Pieters, S. K. Noble, Space weathering on airless bodies. *Journal of Geophysical Research (Planets)* 121, 1865–1884 (2016).
8. B. Hapke, Space weathering from Mercury to the asteroid belt. *Journal of Geophysical Research* 106, 10039 (2001).
9. B. Hapke, *Theory of reflectance and emittance spectroscopy*, Cambridge University Press 469 pages (1993).
10. F. E. DeMeo, R. P. Binzel, S. M. Slivan, S. J. Bus, An extension of the Bus asteroid taxonomy into the near-infrared. *Icarus* 202, 160–180 (2009).
11. F. E. DeMeo, B. Carry, The taxonomic distribution of asteroids from multi-filter all-sky photometric surveys. *Icarus* 226, 723-741 (2013).
12. F. E. DeMeo, B. Carry, Solar System evolution from compositional mapping of the asteroid belt. *Nature* 505, 629–634 (2014).
13. J. R. Masiero, *et al.*, Main Belt Asteroids with WISE/NEOWISE. I. Preliminary Albedos and Diameters. *The Astrophysical Journal* 741, 68 (2011).